JOURNAL OF GEOPHYSICAL RESEARCH, VOL. 91, NO. D8, PAGES 8649–8666, JULY 20, 1986

A Nonisothermal Emissivity and Absorptivity Formulation for Water Vapor

V. RAMANATHAN[1] AND P. DOWNEY

National Center for Atmospheric Research, Boulder, Colorado

This study introduces nonisothermal H_2O emissivity (E) and absorptivity (A) formulations for the troposphere and the stratosphere. The nonisothermal effects arise from the wavelength integration of the Planck function, evaluated at the emitting level temperature (Te), with the monochromatic absorption evaluated at the temperature of the absorbing path (Tp). In general, Te and Tp can differ by as much as 20–50 K in the atmosphere. Most of the published emissivities are essentially isothermal emissivities. We formulate a nonisothermal emissivity that satisfies the constraints posed by the monochromatic form of the transfer equation for a nonisothermal atmosphere. The new formulations employ continuous analytical expressions for E and A that retain the following H_2O radiative properties: the asymptotic properties at small (≈ 0) and large (∞) pathlengths; temperature dependence of line parameters; nonisothermal effects; the e- and p-type continuum in the 500–1200 cm^{-1} region; and the overlap of the e-type continuum with the H_2O line absorption. The E and A expressions are derived from a set of reference 5 cm^{-1} narrow-band calculations for homogeneous atmospheres. When applied to the inhomogeneous atmosphere including arctic, mid-latitude, tropics, and antarctic atmospheres, the cooling rates from 0 to 40 km computed from the emissivity approach agree within 3% of those from the narrow-band calculations; the surface downflux and the upflux at 50 km agree within 1.5%. A major fraction ($>1/2$) of these small errors are due to the strong-line approximation employed in the emissivity model for the 0–800 cm^{-1} and the 1200–2200 cm^{-1} regions, and the emissivity approach itself introduces less than a 1% error in the fluxes. The excellent agreement with the narrow-band calculations essentially verifies the nonisothermal emissivity approach proposed here. We also show that emissivities, fluxes, and cooling rates computed by narrow-band models depend very strongly on the spectral resolution adopted in the model for computing transmittances. Thus the spectral resolution in the narrow-band model is an arbitrary parameter. Furthermore, by comparing the narrow-band model fluxes with line-by-line (LBL) calculations we conclude that the 5 cm^{-1} resolution model underestimates atmospheric opacity due to inadequate treatment of the far wing opacity of lines. We employ a simple continuum-type opacity in our emissivity scheme to bring the present nonisothermal emissivity scheme into excellent agreement with available state-of-the-art LBL calculations.

1. INTRODUCTION

One of the more popular and widely used methods for treating H_2O long-wave radiative effects in climate models is the emissivity approach. However, with the increasing emphasis on the accuracy of the treatment of radiative processes in climate models there is a tendency to lean toward the purely numerical approach in which one precomputes broadband transmissions from line-by-line (LBL) calculations [*Chou and Arking*, 1980] and employs the precomputed values in a table lookup procedure. This approach, while numerically sound, has the considerable disadvantage of dealing with a large set of numbers.

An alternative approach that is also frequently adopted is the narrow-band calculation in which the transmittance is computed in narrow-band intervals employing the *Goody* [1952] or *Malkmus* [1967] random-band models. This is an attractive and sound approach for H_2O. However, in order to make it computationally feasible for climate models the common practice [*Rodgers and Walshaw*, 1966] is to choose a narrow-band interval of 100–150 cm^{-1} which, as shown in this study as well as in the study of *Morcrette and Fouquart* [1985], is too coarse a spectral resolution to yield accurate results. Furthermore, even with a resolution of 100 cm^{-1}, the narrow-band model is computationally slower than the emissivity approach.

The trend towards avoiding the emissivity approach is primarily because of its fundamental limitation, as it is formulated thus far, in accounting for the nonisothermal vertical thermal structure of the atmosphere. Most computed emissivities [e.g., *Staley and Jurica*, 1970; *Sasamori*, 1968; *Ramanathan*, 1976] or empirical emissivities based on laboratory data [*Cess*, 1974; *Manabe and Wetherald*, 1967] are essentially isothermal emissivities. The basic distinction between isothermal and nonisothermal emissivity is as follows: the relevant emissivity for atmospheric flux calculations is the nonisothermal emissivity, in which the temperature used to estimate the Planck function is different from the temperature that governs the transmission. In the isothermal emissivity these two temperatures are assumed to be the same. Some emissivity schemes [e.g., *Ramanathan*, 1976; *Liou and Ou*, 1981, 1983] scale the absorber amount to account for the temperature dependence of the transmission. This procedure is only slightly better than the isothermal emissivity, since it does not account for the temperature dependence of the emissivity that arises from the wavelength integration of the product of the monochromatic absorption and the Planck function. Each of these two functions is evaluated at different temperatures in the transfer equation. Furthermore, the dependence of the absorption on temperature of the absorbing path varies significantly with wavelength and a single universal scaling would seem unlikely to work.

The above mentioned deficiencies of the isothermal emissivity have been recognized in earlier studies [e.g., *Rodgers*, 1967; *Coakley and Briegleb*, 1978; *Garand*, 1983]. However, as yet, we are not aware of any published studies on a self-consistent nonisothermal emissivity formulation. *Rodgers* [1967] considered various forms of emissivity (his E_1 and E_n functions) and concluded that the best approach is numerically to fit emissivities from atmospheric flux calculations. The con-

[1]Now at Department of Geophysics, University of Chicago, Chicago, Illinois.

Paper number 6D0216.
0148-0227/86/006D-0216$05.00

clusions of these earlier studies apply primarily to isothermal emissivities and not to the emissivity approach per se. The accuracy of the emissivity approach was also examined by *Fels and Schwarzkopf* [1975], who concluded that emissivities produce unacceptable errors in cooling rates. *Garand* [1983] has proposed a temperature scaling of the absorbing path to account for nonisothermal effects, and this scheme seems to compare favorably with a coarse spectral resolution (100 cm^{-1}) narrow-band model.

In this paper we demonstrate that it is possible to formulate a nonisothermal emissivity analytically (without resorting to flux calculations) that satisfies the constraints posed by the monochromatic form of the transfer equation for a nonisothermal atmosphere. We then employ this emissivity in a transfer equation and show that the fluxes and cooling rates computed with the emissivity treatment are in excellent agreement with those estimated from a detailed radiation model that computes narrow-band transmission in 5 cm^{-1} intervals. We then demonstrate that the spectral resolution adopted in narrow-band models is an arbitrary parameter, since the emissivities, fluxes, and cooling rates depend very strongly on the adopted spectral resolution. Finally, we make minor adjustments to the emissivity derived from the 5 cm^{-1} narrow-band model and demonstrate that the emissivity approach can yield excellent agreement with LBL calculations. The distinctive feature of the present approach is that it presents a general and formal approach to account for the nonisothermal effects, whereas the earlier schemes [e.g., *Ramanathan*, 1976; *Garand*, 1983] employ ad hoc approaches to obtain the desired accuracy. The new water vapor treatment is incorporated in the National Center for Atmospheric Research (NCAR) community climate model (CCM). The CCM is a spectral general circulation model (GCM) and is described by *Pitcher et al.*, [1983] and *Ramanathan et al.* [1983]. The atmospheric flux calculations are performed for profiles of temperatures and humidities that are representative of observed conditions. However, we also show calculations performed on the CCM three-dimensional grid with the temperature and humidity profiles of the CCM.

2. Emissivity Formulation

2.1. *The Transfer Equation*

The up and down fluxes at any level z can be written as

$$F^{\downarrow}(z) = \int_0^{\infty} B_{\omega}(T_{\infty})A_{\omega}(z, z_{\infty})\, d\omega - \int_z^{z_{\infty}} dz' \int_0^{\infty} L_{\omega}(z, z')\, d\omega \quad (1)$$

$$F^{\uparrow}(z) = B(Ts) + \int_0^{z} dz' \int_0^{\infty} L_{\omega}(z, z')\, d\omega \quad (2)$$

where

$$L_{\omega} = A_{\omega}(z, z')\frac{dB_{\omega}(z')}{dz'}$$

$$B(T) = \int_0^{\infty} B_{\omega}(T)\, d\omega = \sigma T^4 \quad (3)$$

$$B_{\omega}(z') = B_{\omega}[T(z')]$$

and

A_{ω} monochromatic absorption,
ω wavenumber (cm^{-1}),
T temperature,
Ts surface temperature,
T_{∞} temperature of the upper boundary at z_{∞},
z_{∞} reference level for the top of the atmosphere,
$T(z')$ temperature at level z'.

Two assumptions have been made in arriving at (1) and (2): the surface emits as a blackbody, and the solid angle integration is replaced by employing a diffusivity factor of 1.66, according to the suggestion by *Rodgers and Walshaw* [1966]. The monochromatic absorption can be symbolically written as:

$$A_{\omega}(z, z') = A_{\omega}[W(z, z'), P(z, z'), T(z, z')] \quad (4)$$

where W, P, and T are the H_2O amount, the effective broadening pressure and temperature along the path between z and z', respectively. In the narrow-band or emissivity models, scaling approximations are used to represent the continuous variations of P and T along the path with an equivalent homogeneous atmosphere whose pressure and temperature are $\bar{P}$ and $\bar{T}$, respectively.

2.2. *The Transfer Equation: Emissivity Form*

The flux equations (1) and (2) can be written as:

$$F^{\downarrow}(z) = B(T_{\infty})E(z, z_{\infty}) - \int_z^{z_{\infty}} A(z, z')\frac{dB(z')}{dz'}\, dz' \quad (5)$$

$$F^{\uparrow}(z) = B(Ts) + \int_0^{z} A(z, z')\frac{dB(z')}{dz'}\, dz' \quad (6)$$

where, upon comparing the appropriate terms in (5) and (6) with those in (1) and (2), the definitions of E and A can be written as

$$E(z, z_{\infty}) = \frac{\int_0^{\infty} B_{\omega}(T_{\infty})A_{\omega}(z, z_{\infty})\, d\omega}{B(T_{\infty})} \quad (7)$$

$$A(z, z') = \frac{\int_0^{\infty} \{dB_{\omega}(z')/dT(z')^{-1}\}A_{\omega}(z, z')\, d\omega}{dB(z')/dT(z')} \quad (8)$$

The definitions given by (7) and (8) are simply the identities that are required to enable (5) and (6) to be the exact analogues of (1) and (2). The various terms in (5)–(8) have been defined earlier (see the definitions following equation (2)). The E appears as an emission term in (5) and hence we will refer to it as emissivity. In this paper the term A refers to absorptivity, since in the upflux equation this term contributes to a reduction in the upflux, when $dT/dz < 0$. This reduction is due to the net (absorption − emission) absorption of the surface radiation. The approach of employing E and A in the transfer equation is referred to in this paper as the emissivity approach. Equations (5) and (6) are exact analogues of (1) and (2), provided E and A retain the following temperature dependence:

$$E(z, z') = E[W, P, Te, Tp] \quad (9)$$

$$A(z, z') = A[W, P, Te, Tp] \quad (10)$$

In (9) and (10), Te is the emitting level temperature, that is, the temperature at which the Planck functions (B_{ω} and B) are to be evaluated in (7) and (8). Note that $Te = T_{\infty}$ for $E(z, z_{\infty})$. Tp refers to the temperature of the absorbing path $T(z, z')$, which governs the temperature dependence of the absorption A_{ω} (see equation 4)).

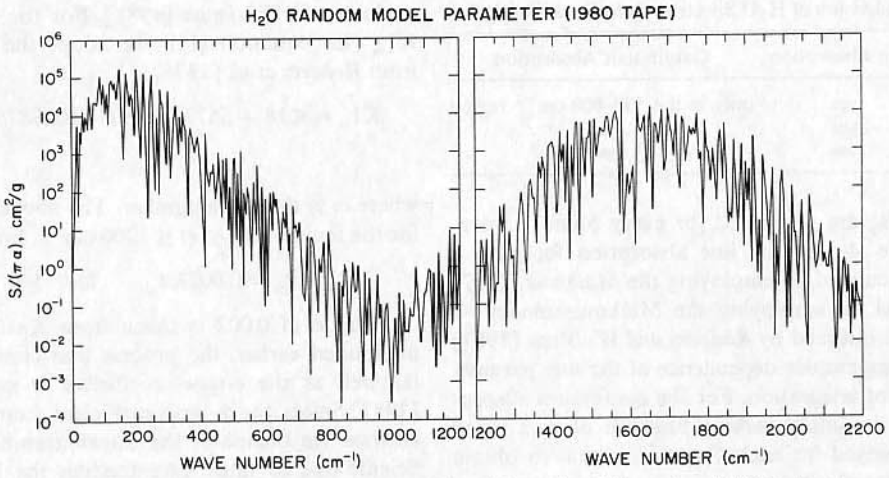

Fig. 1. H_2O random-band model parameter inferred from the 1980 version of AFGL line tape.

Since E (or A) involves integration of A_ω with B_ω (or dB_ω), the dependence of E and A on Te and Tp is governed by the interaction between two nonlinear functions (A_ω and B_ω) of temperature. Each of these two functions are to be evaluated at different temperatures, since, in general, Te is not equal to Tp. In the atmosphere, Te and Tp can differ by as much as 50 K. Next, we will comment on the deficiencies of the isothermal emissivities.

The isothermal emissivities are computed by employing the same temperature for B_ω and A_ω in (7) and (8), which is analogous to letting $Te = Tp$ in (9) and (10). When these isothermal emissivities are subsequently employed in (5) and (6), ambiguity arises as to which of the two temperatures, that is, Te or Tp should be employed in the emissivity expression. This ambiguity is avoided in some emissivity schemes (for example, *Sasamori* [1968]; *Ramanathan* [1976]; *Liou and Ou* [1981], to cite a few) by scaling the absorber amounts with the temperature-dependent line parameters. This procedure of scaling the absorber amount does not account for the temperature dependence of E and A that arises from the wavelength integration of the product of B_ω and A_ω. In summary, there are no analogues between the isothermal emissivity (with or without the temperature-scaled pathlength) and the emissivity formulation that is appropriate for the flux equation.

By partial integration of the kernel in the integrals of (1) and (2), the kernel L_ω can also be expressed in terms of B_ω dA_ω, and an emissivity that is consistent with this kernel can be derived (see equation 3 of *Rodgers* [1967]). But the resulting emissivity expression (E_2 of *Rodgers* [1967]) is considerably more complicated than (7) or (8), since it involves an integral over the path length (z to z') and also does not have an analogue to the homogeneous emissivity. Equations (7) and (8), on the other hand; involve an integration over only the wavelength. Hence as we will demonstrate later, the E and A can be precalculated for homogeneous paths and can subsequently be applied in the transfer equation.

The parameterization of E and A, based on the conceptual framework given in (9) and (10), requires reference emissivities and reference calculations of fluxes and cooling rates which are described next. The parameterization of emissivities is undertaken in two steps:

Step 1. A 5 cm^{-1} narrow-band model is used to compute reference emissivities and absorptivities for homogeneous atmospheres as a function of H_2O amount W, total pressure P, and the two temperatures Te and Tp (see equations (9) and (10)). Nonisothermal emissivity expressions are fit to these reference emissivities. The fluxes and cooling rates for inhomogeneous atmospheric profiles, as computed by the narrow-band and the emissivity models, are compared. The objective of step 1 is to demonstrate that the present nonisothermal emissivity approach can retain the accuracy of more detailed calculations with respect to fluxes and cooling rates.

Step 2. In this step we modify the parameterized emissivity to account for the contributions of far wings of rotational lines that are not adequately treated in a 5 cm^{-1} narrow-band model. We adopt available line-by-line calculations of atmospheric fluxes to arrive at a very simple continuum-type transmission within the context of the emissivity approximation. It would have been simpler and straightforward to adopt line-by-line calculations for the reference emissivities, but such calculations are not available. However, as we will show later, not much is sacrificed by using a narrow-band model for step 1. It is important to note that the procedure outlined in this paper for developing nonisothermal emissivities from detailed calculations is not restricted to narrow band reference calculations.

2.3. *Reference Emissivities*

H_2O has a rich spectrum of rotation and vibration-rotation lines spanning the entire long-wave region from 0 to 2200 cm^{-1}. Figure 1 shows the distribution of line intensities (averaged over 5 cm^{-1} wave number interval) obtained from the Air Force Geophysics Laboratory (AFGL) line data [*Rothman*, 1981]. In addition to the lines, H_2O also has continuum features. The source for this continuum is still being debated (for example, see *Burch* [1982]), but the absorption coefficient seems to be better understood [*Roberts et al.*, 1976]. However, the magnitude of the coefficient is subject to large uncertainties (see discussions later in this section). Hence the continuum is frequently referred to as the "empirical continuum" (for example, see *Burch* [1982]) and the absorption coefficient is inferred from laboratory or atmospheric measurements. The continuum absorption coefficient, K_ω is normally written as the sum of two terms:

$$K_\omega = K1_\omega e + K2_\omega P \tag{11}$$

where e is the H_2O partial pressure and P is the atmospheric pressure and $K1_\omega$ and $K2_\omega$ are referred to as the e-type and the p-type absorption, respectively.

The reference emissivities are calculated as follows. The

TABLE 1. Subdivision of H_2O Spectrum Into Broadbands

Spectral Region	Line Absorption	Continuum Absorption
0–800	yes	only in the 500–800 cm^{-1} region
800–1200	yes	yes
1200–2200	yes	no

values of A_ω and B_ω are computed for every 5 cm^{-1} wavelength interval. The A_ω for the line absorption for each 5 cm^{-1} interval is calculated by employing the *Malkmus* [1967] random-band model. In employing the Malkmus model we adopt the procedure outlined by *Rodgers and Walshaw* [1967] for including the temperature dependence of the line parameters along the path of integration. For the continuum absorption, since K_ω is a smoothly varying function of ω, a mean value of K_ω is employed for each 5 cm^{-1} interval to obtain the narrow band transmission.

Our choice of 5 cm^{-1} was motivated by the *Kiehl and Ramanathan* [1983] study. That study considered various intervals ranging from 5 to 50 cm^{-1} for the CO_2 15-μm bands and concluded that the 5 cm^{-1} resolution yielded the best agreement with the laboratory data for CO_2 band absorption. *Kiehl and Ramanathan* [1983] also demonstrated that coarsening the interval to values in excess of 25 cm^{-1} leads to a significant overestimation of the absorption for CO_2 and, as will be shown later, the same conclusion applies for H_2O. In each of the 5 cm^{-1} intervals, H_2O has at least 25 lines and significantly more in most of the intervals.

The above results for CO_2 do not necessarily imply that a 5 cm^{-1} interval would also be appropriate for H_2O. In particular, the far wing contributions, which are potentially more important for H_2O than CO_2, are not adequately accounted for in a narrow spectral interval model. However, as we show later, the far wing contributions (which are poorly known because of the uncertainty in line shapes) can be included through a continuum-type absorption.

2.4. *Spectroscopic Data*

The random-band model parameters for the rotational lines (including their temperature dependence) were obtained from the 1980 version of the AFGL atmospheric absorption line parameters [*Rothman*, 1981]. The modification as well as the refinements that were incorporated in the 1980 version are explained by *Rothman* [1981]. For the continuum coefficient $K1_\omega$ (see equation (11)) we adopt the following expression from *Roberts et al.* [1976]:

$$K1_\omega = 4.18 + 5577.8 \exp(-0.00787\omega) \qquad [\text{g cm}^{-2}]^{-1} \tag{12}$$

where ω is the wave number. The above expression is applied for the region $500 \le \omega \le 1200$ cm^{-1}. For $K2_\omega$ we let:

$$K2_\omega = 0.002K1_\omega \qquad \text{for} \quad 500 \le \omega \le 1200 \tag{13}$$

The value of 0.002 is taken from *Kneizys et al.* [1980]. As mentioned earlier, the process that contributes to the *p*-type (as well as the *e*-type) coefficient is not known yet. *Burch* [1982] infers the *p*-type coefficient from laboratory data, as follows. He computes the transmittance (or absorption coefficient) due to lines by extending the Lorentz shape up to about 20 cm^{-1} from line center. He then compares this transmittance with the measured transmittance and infers a *p*-type coefficient that will match the data. Burch's estimate for the ratio $(K2_\omega/K1_\omega)$ varies from about 0.001 at 1000 cm^{-1} to about 0.01 at 500 cm^{-1}. However, the ratio $(K2_\omega/K1_\omega)$ is very sensitive to the assumed line profile [*Burch*, 1982]. Obviously, there is a large range of uncertainty and the major source of uncertainty arises from lack of understanding of the line shape beyond a few wave numbers from the line center.

For the spectral regions $0 \le \omega < 500$ cm^{-1} and $1200 < \omega \le 2200$ cm^{-1}, the continuum absorption coefficients are more uncertain than the uncertainty quoted earlier for the $500 \le \omega \le 1200$ cm^{-1} region. Hence we have not included the continuum for $\omega < 500$ cm^{-1} and for $\omega > 1200$ cm^{-1}.

2.5. *Analytical Formulation for E and A*

The H_2O long-wave absorption is subdivided into three broad spectral regions, as shown in Table 1. In this spectral region, between 0 to 800 cm^{-1}, the continuum absorption is included only for the 500–800 cm^{-1} region. This subdivision facilitates the treatment of overlapping absorption by the lines and the continuum as well as the effects of overlap between H_2O absorption and that of other trace gases. The basic concepts of the formulation are described below. Details of the parametric expression and the numerical constants are given in the appendix. First, we will describe the formulation for line

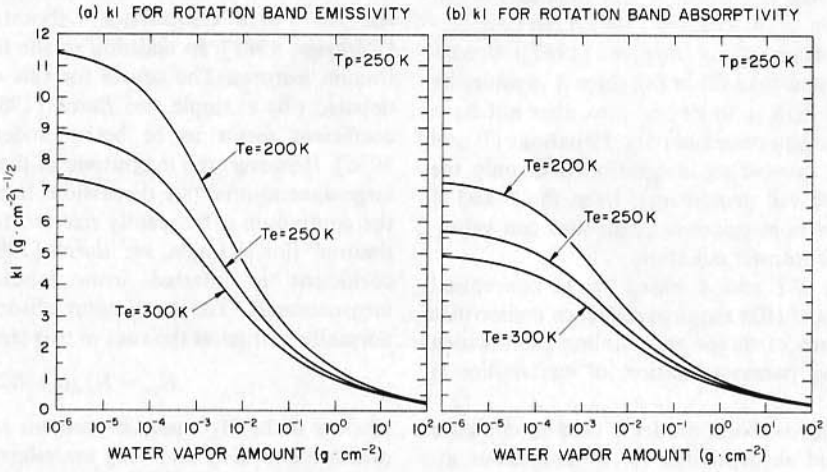

Fig. 2. The Planck-weighted effective absorption coefficient *kl*. The curves show the dependence on the emitting level temperature *Te*. *Tp* is the path length temperature.

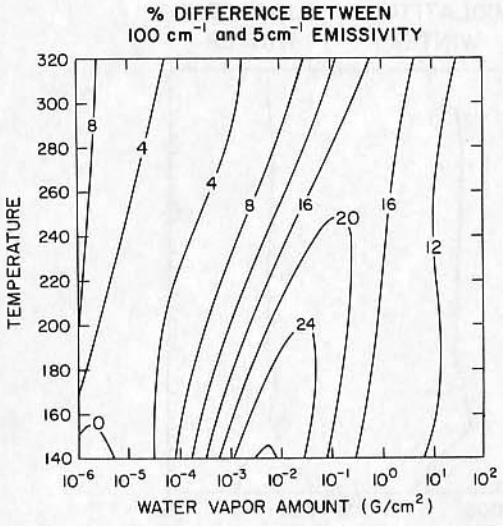

Fig. 3. Percent difference between emissivity computed with a 100 cm^{-1} and a 5 cm^{-1} random-band model. The water vapor amount is the pressure-weighted amount.

absorption in the 0–800 cm^{-1} and the 1200–2200 cm^{-1} regions, which are the rotation and the vibration-rotation bands, respectively.

Rotation and vibration-rotation bands. The strong-line approximation will be invoked, since, as will be shown later, this is an excellent approximation for these two bands. In the strong-line approximation, the narrow-band absorption a_i, in the interval i (whose width is 5 cm^{-1}), can be written as

$$a_i = 1. - \exp\left[-(1.66 k_i \beta_i U)^{1/2}\right] \tag{14}$$

where

$$U = \int (P/P_0)\, dW \text{ g cm}^{-2} \tag{15}$$

and k_i and β_i are the line strength and line structure parameters of the random-band model, and these parameters depend on the path length temperature Tp. In (15), $P_0 = 1$ atm. As is obvious from (14), the strong-line approximation enables us to treat the path length dependence on W and P in terms of the single variable U. Upon inserting (14) in place of A_ω in (7), the reference emissivity E(REF) can be written as

$$E(\text{REF}) = \left[\sum_{i=1}^{N} B_i(Te) a_i\right] \Big/ B(Te) \tag{16}$$

where N is the number of 5 cm^{-1} intervals for the band under consideration, i denotes the spectral interval, and a_i is defined in (14). The E(REF) is calculated for U ranging from 10^{-6} to 10^4 in grams per square centimeter and for Te and Tp ranging from 160 to 320 K. The calculations include cases for which $Te = Tp$ and $Te \neq Tp$. The procedure adopted to parameterize A from A(REF) is identical to that adopted for E, and hence only the formulation for E will be described.

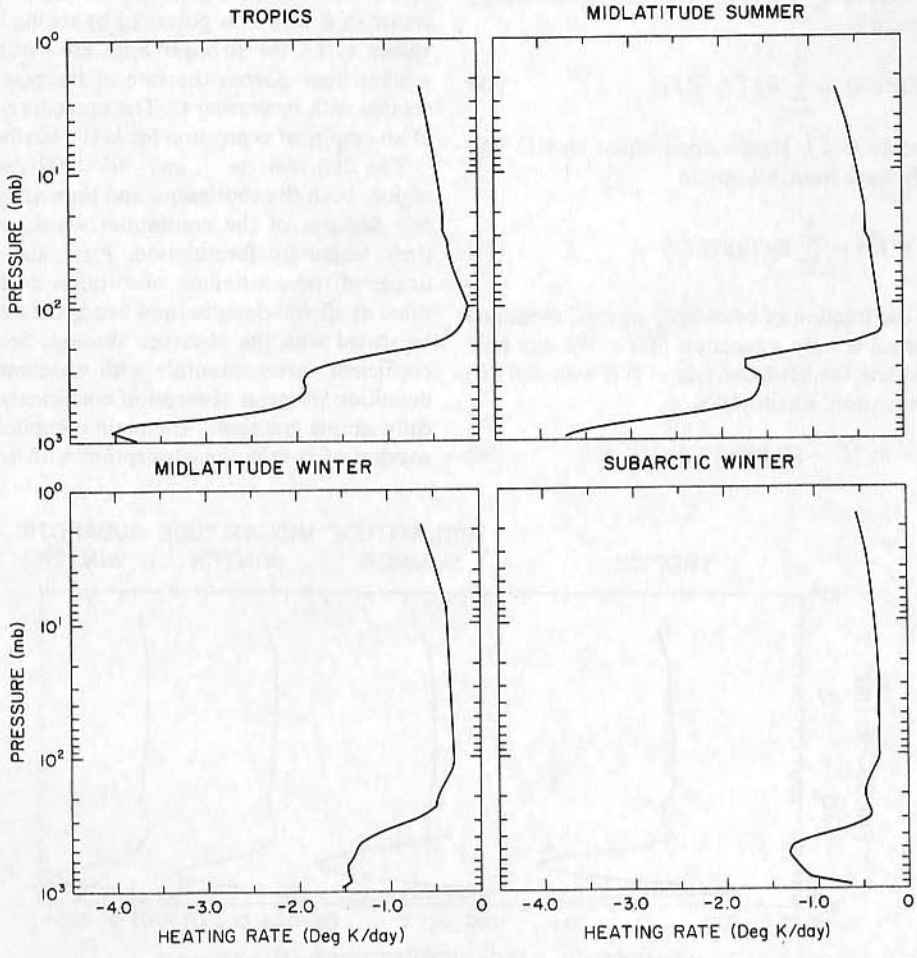

Fig. 4. Long-wave heating rate computed with the Malkmus narrow-band model with 5 cm^{-1} resolution, that is, NBM/M.

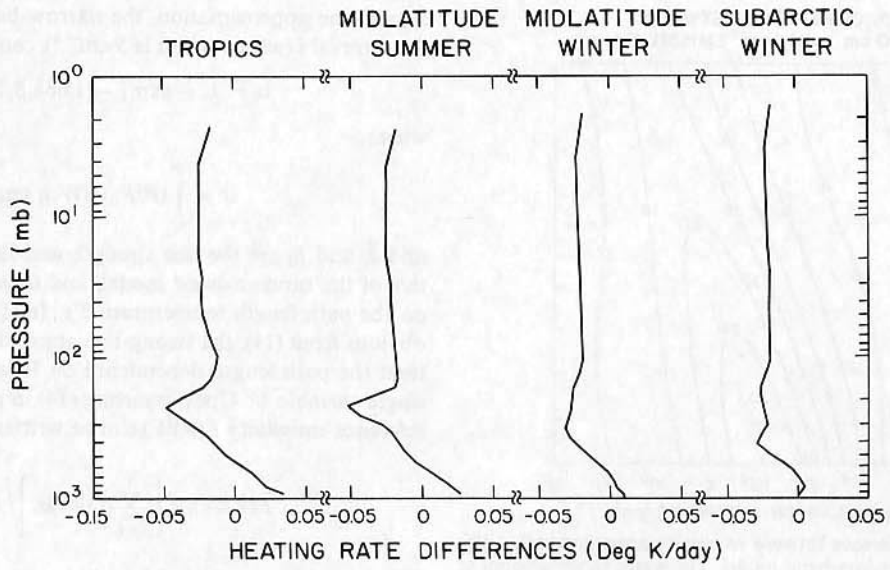

Fig. 5. The error in heating rate due to the strong-line approximation. The figure shows the difference between NBM/S and NBM/M.

We express the parameterized emissivity E as

$$E = f[1. - tl] \qquad tl = \exp(-klU^{1/2}) \tag{17}$$

The parameters f and kl are obtained from E(REF), as described below. The optically thick limit is employed to solve for f. In this limit, that is, $U \gg 1$, (14) yields $a_i \approx 1$ and letting $a_i = 1$ in (16), we obtain:

$$E(\text{REF}) \approx \sum_{i=1}^{N} B_i(Te)/B(Te) \tag{18}$$

For $U \gg 1$, (17) yields $E \approx f$. Hence upon equating (16) and (17) for the optically thick limit, we obtain

$$f(Te) = \sum_{i=1}^{N} B_i(Te)/B(Te) \tag{19}$$

Note first that f is the fraction of blackbody energy contained in the band and hence is only a function of Te. We can now solve for kl by replacing the left-hand side of (17) with E(REF) and inverting this equation, which yields

$$kl = -\ln\{1. - [E(\text{REF})/f]\}/(U^{1/2}) \tag{20}$$

The effective absorption coefficient kl depends on Te, Tp, and U. The dependence of kl on U is shown in Figure 2 for the rotation band. We show kl for emissivity (Figure 2*a*) and absorptivity (Figure 2*b*) separately to highlight the fact that separate kls are needed for E and A. As seen from Figure 2, kl decreases with increasing U. For small path lengths the increase of E with U is governed by strong lines, while for larger values of U, the stronger lines are saturated and hence the weaker lines govern the rate of increase of E. Hence kl decreases with increasing U. The procedure adopted for arriving at an empirical expression for kl is described in the appendix.

The 500–800 cm^{-1} and 800–1200 cm^{-1} region. In this region, both the continuum and lines are important. There are two features of the continuum which considerably simplify their emissivity formulation. First, the temperature dependence of the continuum absorption coefficient is nearly the same at all wavelengths, and hence the dependence on Tp can be scaled with the absorber amount. Second, the absorption coefficient varies smoothly with wavelength, which facilitates definition of mean absorption coefficients in terms of analytically simple functions. The main complication arises from the overlap of continuum absorption with rotational lines. Con-

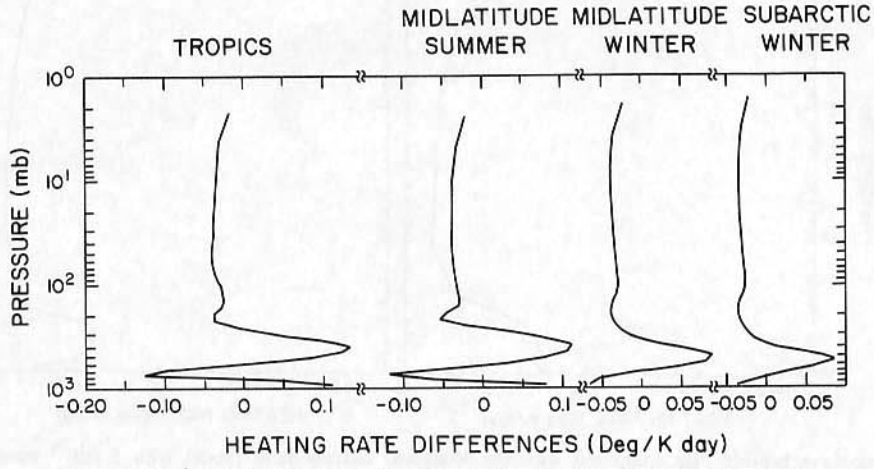

Fig. 6. The difference in heating rate between the emissivity model and NBM/M.

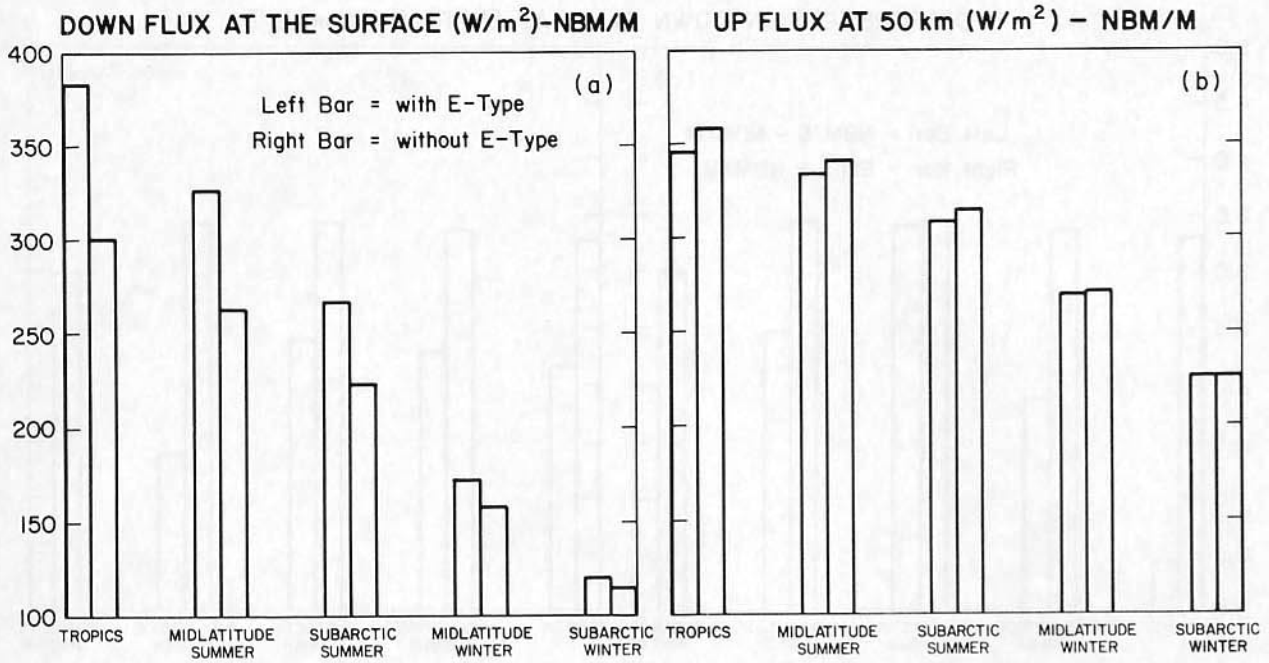

Fig. 7. (*a*) Computed downflux at the surface and (*b*) upflux at 50 km. The model is NBM/M, that is, the narrow-band Malkmus model.

sidering first the continuum without line overlap, the continuum emissivity can be expressed as

$$E = f\left\{\sum_{i=1}^{2} 0.5[1 - tc(i)]\right\} \tag{21}$$

$$tc(i) = \exp\,[-kc(i)(Y + C1U] \tag{22}$$

$$kc(1) = \overline{kc} \tag{23}$$

$$kc(2) = 2\overline{kc} \tag{24}$$

$$\overline{kc} = F(Y)(2/3)\left\{\left[\int_{\Delta\omega} K1_\omega B_\omega\, d\omega\right]\Big/\left[\int_{\Delta\omega} B_\omega\, d\omega\right]\right\}1.66 \tag{25}$$

$$Y = \int \exp\left\{1800\left[\frac{1}{Tp} - \frac{1}{296}\right]\right\} e\, dW \tag{26}$$

For the $500 \le \omega \le 800$ cm^{-1} region

$$C1 = 0.0017$$
$$F(Y) = [1. + 2Y]/[1. + 15Y] \tag{27}$$

For the $800 < \omega < 1200$ cm^{-1} region

$$C1 = 0.002$$
$$F(Y) = 1. \tag{28}$$

In (21), f has been defined earlier in (19). As implied in (21), each of the two regions is divided into two subregions and the Planck-weighted absorption coefficient kc in one of the subregions is twice the other, which yields the consistency relation given in (25). We chose the parametric form of $kc(2) = 2kc(1)$ for computational speed, since $tc(2) = [tc(1)]^2$. Note also that, as opposed to the coefficient kl for the rotation and vibration-rotation bands which depends on Te and Tp, kc depends only on Te. The value kc is independent of Tp because the Tp dependence of the monochromatic absorption coefficient $k1_\omega$ is the same for all spectral regions and, as a result, the dependence on Tp can be scaled with the path length, as shown in (26). The value $\overline{kc}$ is evaluated from (25), where a 5 cm^{-1} interval is used to evaluate the spectral integration. The parametric expression for $\overline{kc}$ is given in the appendix. In principle, $C1$, given in (27), should be 0.002. However, the factor 0.0017 gives better agreement with the reference model. The line absorption in the 500–800 cm^{-1} region has been included in the definition of the pure rotation band emissivity. Hence the overlapping of the rotational lines with the continuum absorption is treated by modifying (21), as follows:

$$E = f\sum_{i=1}^{2} \{0.5tl(i)[1 - tc(i)]\} \tag{29}$$

$$tl(i) = \exp\,[-kl(i)(U^{1/2})] \tag{30}$$

The expression for $kl(i)$ is given in the appendix. For the 800–1200 cm^{-1} region, since the line absorption has not been included thus far, the emissivity given by (21) is modified as follows:

$$E = f\left\{\sum_{i=1}^{2} 0.5[1 - tl(i)tc(i)]\right\} \tag{31}$$

The lines in this region are sufficiently weak that the strong-line approximation will not hold. Hence we employ the complete Malkmus model expression, with the result that the emissivity depends on U as well as on W (see Table A2). The random-model parameters are obtained for 200 cm^{-1} intervals and are subsequently scaled with path length dependent correction factor (see equations (10) to (12) in Table A2 in the appendix) to yield excellent agreement (within 0.1%) with fluxes computed for the 800–1200 cm^{-1} region with a 5 cm^{-1} model. Results for the fluxes in this spectral region are quoted in section 2.6.

2.6. *Empirical Correction Terms for Far Wing Absorption*

The procedure described thus far completes Step 1 (see description under section 2.2) of the parameterization, which concerns the development of an emissivity scheme based on

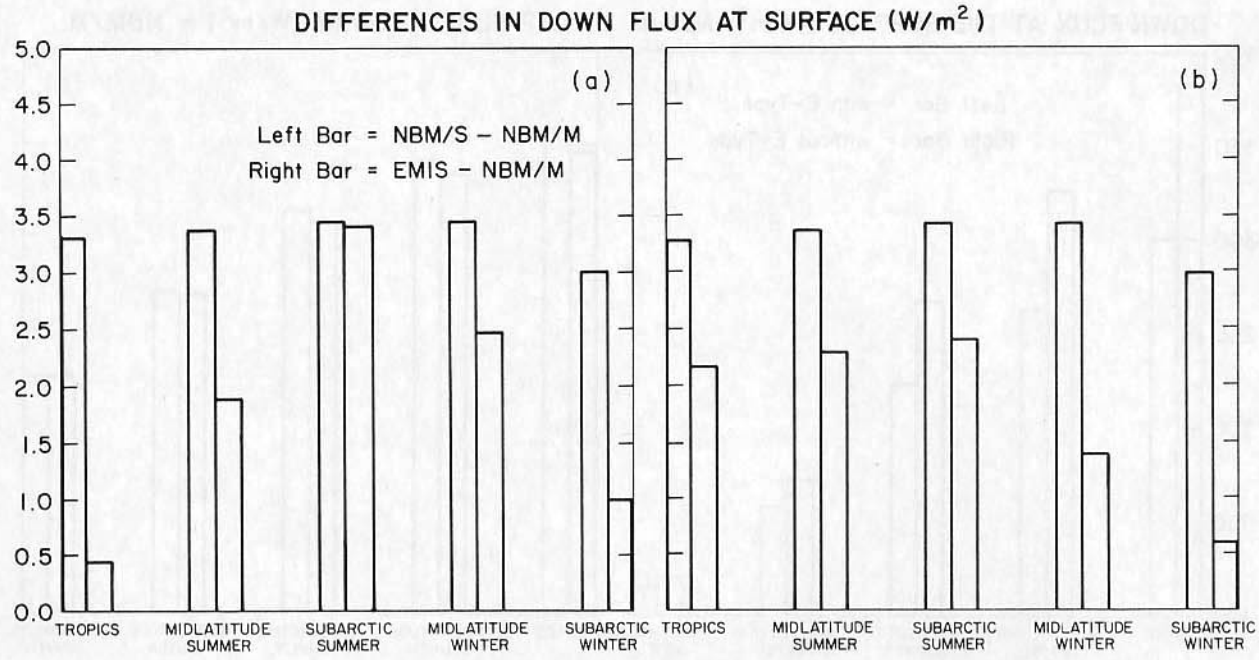

Fig. 8. Difference in the downflux between NBM/S and NBM/M (left bar) and between EMIS and NBM/M (right bar). (*a*) Includes *e*-type continuum. (*b*) Does not include the *e*-type continuum.

the reference narrow-band model. The emissivities, fluxes, and cooling rates obtained from this emissivity scheme will be compared with those estimated from the narrow-band model to demonstrate the validity of the approach proposed in this study. However, as will be shown later (in section 4.4), the 5 cm^{-1} narrow-band model underestimates the atmospheric opacity when compared with LBL calculations. Furthermore, it will be shown later that this deficiency is attributable to the inadequate treatment of the far wing effects in the 5 cm^{-1} narrow-band model. In order to rectify this deficiency in the emissivity scheme, the line transmission, as given by (17) and (30), is modified to:

$$tl = \exp\,[-kl[(U^{1/2}) + G\,U] \tag{32}$$

where for the 0–800 cm^{-1} and 1200–2200 cm^{-1} regions,

$$G = 0.1 + \frac{0.3}{1. + 4.5U} \tag{33}$$

and for the 500–800 cm^{-1} region,

$$G = 0.26 + \frac{0.78}{1. + 4.5U} \tag{34}$$

The variables $k1$ and U retain their previous definition. The added term, that is, GU, is conceptually similar to a continuum-type opacity that arises from far wings of rotational lines, and this added transmission brings the emissivity scheme to an excellent agreement with LBL calculations. We

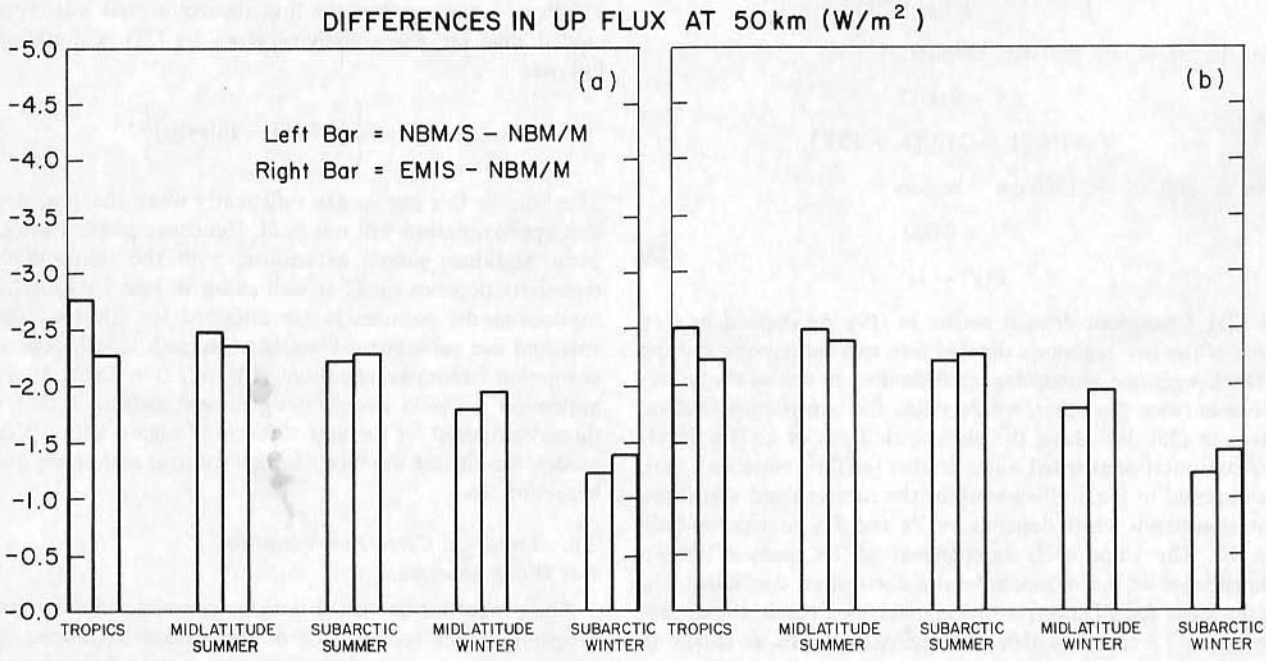

Fig. 9. Same as Figure 8 but for upflux at 50 km.

TABLE 2a. Downflux at the Surface, Including *e*-Type and *p*-Type Absorption

Atmosphere	Model		
	NBM/M	NBM/S	EMIS
Tropics	383.24	386.53	383.68
Mid-latitude summer	326.59	329.96	328.47
Subarctic summer	267.39	270.83	270.80
Mid-latitude winter	172.58	176.03	175.05
Subarctic winter	119.55	122.55	120.53

Downflux is in watts per square meter. Far wing effects are not included. NBM/M, narrow-band model/Malkmus expression; NBM/S, narrow-band model/strong-line approximation; EMIS, emissivity scheme.

also note that the far wing transmission correction is not applied to the 800–1200 cm^{-1} region for the following reason: the lines in this region are sufficiently weak that the 5 cm^{-1} NBM/M model is in good agreement with the line-by-line calculations. For example, for the mid-latitude summer atmosphere profile, the downward flux in the 800–1200 cm^{-1} region yielded by the narrow-band Malkmus (NBM/M) model is 13.04 W m^{-2}, and that yielded by the emissivity (EMIS) model is 12.8 W m^{-2}, whereas LBL calculations of A. Arking (private communication, 1985) yield 14.49 W m^{-2}. This small error of about 1.5 W m^{-2} would be minimized further with the inclusion of the *e*-type continuum.

3. Comparison of Homogeneous Emissivity and Absorptivity

3.1. *Comparison With Reference Emissivities*

For all ranges of temperatures and path lengths of relevance to the atmosphere, the parameterized emissivity agrees within 2% with the reference emissivities. Recall that the reference emissivities (for all bands) are computed from a narrow-band model with a spectral resolution of 5 cm^{-1}. The maximum difference of about 2% could have been further reduced if we had resorted to higher-order polynomials. In view of the uncertainties in line parameters of the order of 15% [*Rothman et al.*, 1983], we considered it unnecessary to attempt a more accurate fit to the reference emissivities. The error of 2% or less in the homogeneous emissivities basically contributes to the 3% error in cooling rates (discussed in section 3.2).

3.2. *Comparison With Published Emissivities*

For the H_2O path lengths relevant to the atmosphere there were substantial differences between the published emissivities and the present reference emissivities. For example, the reference emissivity (without the continuum) differed by as much as 30% with *Sasamori* [1968]; by about 25% with *Rodgers and Walshaw*'s [1966] 16-band model version; by about 20% with that of *Ramanathan* [1976] and *Staley and Jurica* [1970]. These differences are the maximum differences and do not occur for all *U*s and *T*s. Furthermore, the earlier emissivities are larger than the present values. One feature that is common to all the earlier calculations is that these are based on coarse spectral resolution data: *Rodgers and Walshaw* [1966] adopt 100 cm^{-1} resolution; *Ramanathan*'s [1976] emissivity is based on *Staley and Jurica*'s [1970] calculated emissivity which employs 40 cm^{-1} resolution; *Sasamori*'s [1968] spectral resolution is not given. Hence we discuss next the effect of spectral resolution on the computed emissivity.

TABLE 2b. Upflux at 50 km

Atmosphere	Model		
	NBM/M	NBM/S	EMIS
Tropics	346.19	343.41	343.91
Mid-latitude summer	334.7	332.21	332.34
Subarctic summer	309.1	306.87	306.81
Mid-latitude winter	270.53	268.74	268.58
Subarctic winter	226.68	225.45	225.29

Upflux is in watts per square meter. Far wing effects are not included. NBM/M, narrow-band model/Malkmus expression; NBM/S, narrow-band model/strong-line approximation; EMIS, emissivity scheme.

TABLE 3a. Downflux at the Surface Due to *e*-Type Absorption

Atmosphere	Model	
	NBM/M	EMIS
Tropics	82.23	80.54
Mid-latitude summer	63.15	62.77
Subarctic summer	43.53	44.56
Mid-latitude winter	14.58	15.7
Subarctic winter	5.05	5.46

Downflux (in watts per square meter) was obtained by taking the difference in the downflux between two calculations, one with and the other without *e*-type continuum. See Table 2a for explanation of the models mentioned. Far wing effects are not included.

3.3. *Effect of Spectral Resolution on the Computed Emissivity*

Figure 3 shows the percent difference between the emissivity computed with a 100 cm^{-1} resolution and that computed with the 5 cm^{-1} resolution model. All of the emissivities are computed for 1 atm pressure. As seen from Figure 3, coarsening the spectral resolution leads to a substantial overestimation of the emissivity. This tendency is obvious in view of the significant spectral variation of line strengths over 100 cm^{-1} intervals (see Figure 1). Spectral averaging of line strengths (over 100 cm^{-1} intervals) that vary by more than an order of magnitude within the averaging interval would lead to an overestimation of the mean opacity. The effect of spectral resolution on fluxes and cooling rates are discussed in section 4.

4. Comparison of Fluxes and Cooling Rates

The accuracy of the emissivity approach is examined by comparing fluxes and cooling rates computed with the emissivity scheme with those computed from a narrow-band model. Two versions of the narrow-band model are employed.

TABLE 3b. Same as Table 3a but for Upflux at 50 km

Atmosphere	Model	
	NBM/M	EMIS
Tropics	−12.84	−12.92
Mid-latitude summer	−7.28	−7.28
Subarctic summer	−6.07	−6.14
Mid-latitude winter	−1.25	−1.29
Subarctic winter	−0.15	−0.16

Upflux is given in watts per square meter. See footnotes for Table 3a.

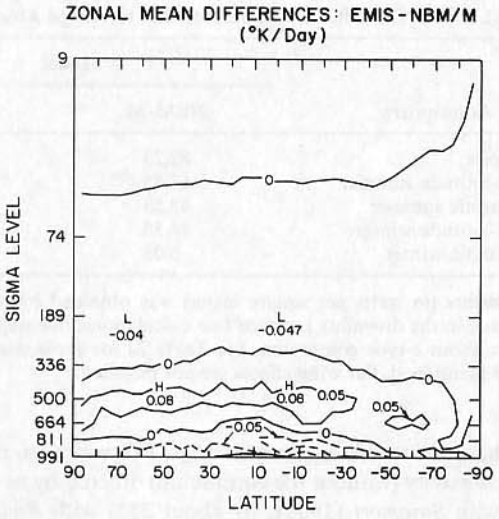

Fig. 10. The zonal mean difference in radiative-heating rate between EMIS and NBM/M. These calculations are performed in the GCM grid, consisting of 40 latitude points and 48 longitude points for each latitude. The negative latitude points refer to the southern hemisphere. The temperature and humidity values are taken from day 200 of a January simulation by the model.

The first version, referred to as NBM/M, computes narrow-band transmittances of rotational lines by adopting the Malkmus random band model [*Malkmus*, 1967]. The second version, referred to as NBM/S, employs the strong-line approximation for computing line transmittances in the 0–800 cm^{-1} and 1200–2200 cm^{-1} regions. However, both versions adopt the Malkmus model for the lines in the 800–1200 cm^{-1} region. Both versions employ (1) the same narrow-band spectral width of 5 cm^{-1}, (2) the same treatment for continuum absorption, and (3) the same line parameters. Furthermore, the line parameters are identical to those adopted for deriving the emissivity scheme, and the same finite-difference scheme was used to compute the flux integrals. Furthermore, the emissivity scheme employs the same finite difference scheme as that of the NBM model and an identical procedure for prescribing the vertical distribution of temperatures and humidities. The scaled path length temperature Tp is computed by letting $Tp = \int T\, du / \int du$.

In view of the above similarities, the comparison study will accomplish the following objectives: (1) The comparison of the two versions of the narrow-band model will illustrate the accuracy of the strong-line approximation; (2) The comparison of the emissivity scheme with the NBM/S model will illustrate the validity of the emissivity approach; and (3) The comparison of the emissivity scheme with the NBM/M model will illustrate the overall accuracy of the emissivity scheme.

It should be noted that when comparing with narrow-band models, the far wing effects are removed from the emissivity model. The computations employ 30 vertical levels between the surface and 1 mbar and adopt profiles of temperatures and pressures as given by *McClatchey et al.* [1972]. For H_2O the McClatchey et al. profile is adopted from the surface to 12 km. Above 12 km the H_2O mixing ratio is assumed to be 3 ppm (by mass). Five atmospheric profiles are included for the comparison study, which (in the terminology of McClatchey et al.) are: tropics, mid-latitude summer, subarctic summer, mid-latitude winter, and subarctic winter. These five profiles are representative of observed values for the respective seasons and latitudes.

After demonstrating the validity of the emissivity approach, we compare the NBM and emissivity models with LBL calculations to bring out some basic deficiencies in NBM models. We then show that these deficiencies can easily be corrected by the far wing correction proposed in section 2.6.

4.1. *Accuracy of the Strong-Line Approximation*

For reference purposes the radiative-heating rates computed from the narrow band Malkmus (NBM/M) model are shown in Figure 4. The differences in the heating rates between the two versions of the narrow-band model, that is, NBM/S − NBM/M, are shown in Figure 5. These differences illustrate the heating rate errors due to the strong-line approximation in the pure rotation (0–800 cm^{-1}) and the vibration-rotation (1200–2200 cm^{-1}) bands. The strong-line approximation underestimates the long-wave cooling in the lower troposphere and overestimates it in the rest of the atmosphere. However, the maximum error, which occurs around 200 mbar, is only −0.05 K/day. Overall, Figure 5 leads to the conclusion that the strong-line approximation is an excellent approximation for the troposphere and the stratosphere. This conclusion is in agreement with that of *Rodgers and Walshaw* [1966].

4.2. *Accuracy of the Emissivity Scheme*

The differences in the heating rates between the emissivity scheme and the narrow-band model (without the strong-line approximation) are shown in Figure 6. On a percentage basis, for all of the profiles shown in Figure 6, the troposphere/stratospheric heating rates from the emissivity scheme agree with those from the reference calculations within 3%. In absolute magnitude the maximum difference of about 0.12

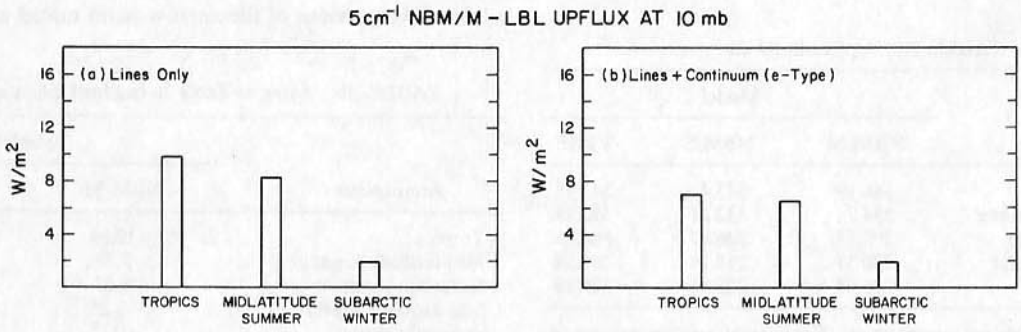

Fig. 11. Difference in the upflux at 10 mbar between NBM/M and line-by-line calculations of A. Arking (private communication, 1985). (*a*) Includes only lines. (*b*) Includes lines and *e*-type continuum.

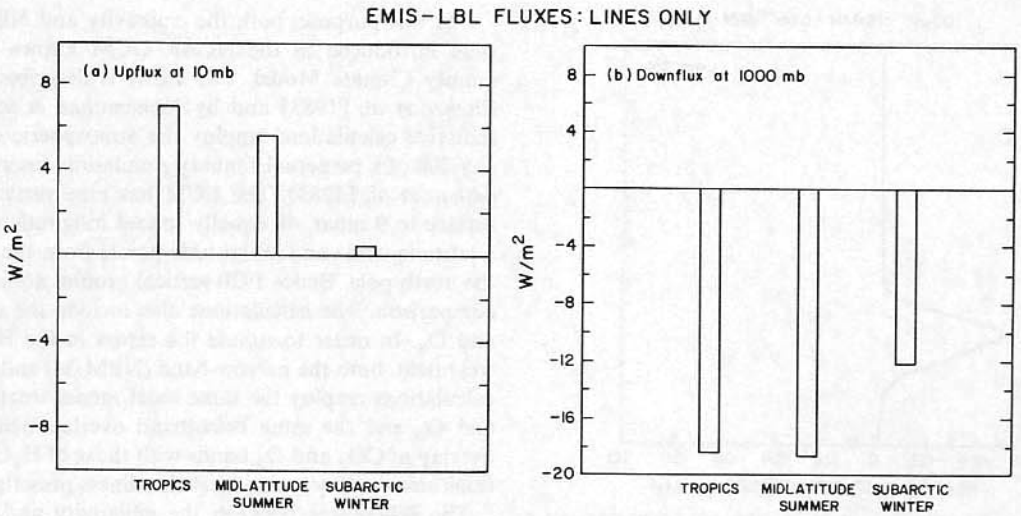

Fig. 12. Difference in fluxes between EMIS and line-by-line calculations of A. Arking (private communication, 1985). The EMIS model does not have far wing effects. (*a*) Upflux at 10 mbar. (*b*) Downflux at 1000 mbar.

K/day occurs in the surface layer for the tropics profile, but note from Figure 3 that the cooling rate in this region is about 4 K/day. The agreement in the stratosphere (from 100 to 2 mbar) is excellent, being within 0.03 K/day of the narrow-band model. As seen from Figure 5, roughly 0.02 K/day of the 0.03 K/day difference shown in Figure 6 is due to the strong-line approximation.

The computed downfluxes and upfluxes for the NBM/M model are shown in Figure 7. The differences in the downfluxes at the surface between NBM/S and NBM/M and between EMIS and NBM/M are shown in Figure 8*a* for the case with *e*-type absorption and in Figure 8*b* for the case without *e*-type absorption. The corresponding differences for the upflux at 50 km are shown in Figures 9*a* and 9*b*. For each of the atmospheres shown in Figures 8 and 9, the left bar is the difference between the two versions of the narrow-band model and hence illustrates the error due to the strong-line approximation. The right bar is the difference between the emissivity scheme and the Malkmus model. Hence subtraction of the left bar from the right bar would indicate the error in the emissivity approach. Furthermore, Figures 8*b* and 9*b* indicate the error in the treatment of rotational lines. Subtraction of the errors shown in Figure 8*b* (or 9*b*) from those shown in Figure 8*a* (or 9*a*) illustrates the error in the treatment of the *e*-type absorption as well as its overlap with the rotational lines. The values of the surface downflux and the upflux at 50 km are also shown in Tables 2*a* and 2*b*. The effect of the *e*-type absorption on the fluxes is shown in Tables 3*a* and 3*b*. With the above background information the following inferences can be drawn from Figures 8 and 9 and Tables 2 and 3.

1. For the downward flux due to rotational lines (Figure 8*b*) the error in the emissivity scheme is within 3 W m^{-2}.
2. However, roughly 60% of the error is due to the strong-line approximation (compare the left bar with the right bar in Figure 8*b*).
3. Similar conclusions apply to the upflux at 50 km.
4. Hence the emissivity approach, by itself, introduces a negligible (<0.5 W m^{-2}) error.
5. Upon comparing the right bars in Figures 9*a* and 9*b*, it is seen that introduction of the *e*-type absorption does not introduce additional errors in the upflux.
6. For the surface downward flux the emissivity approach

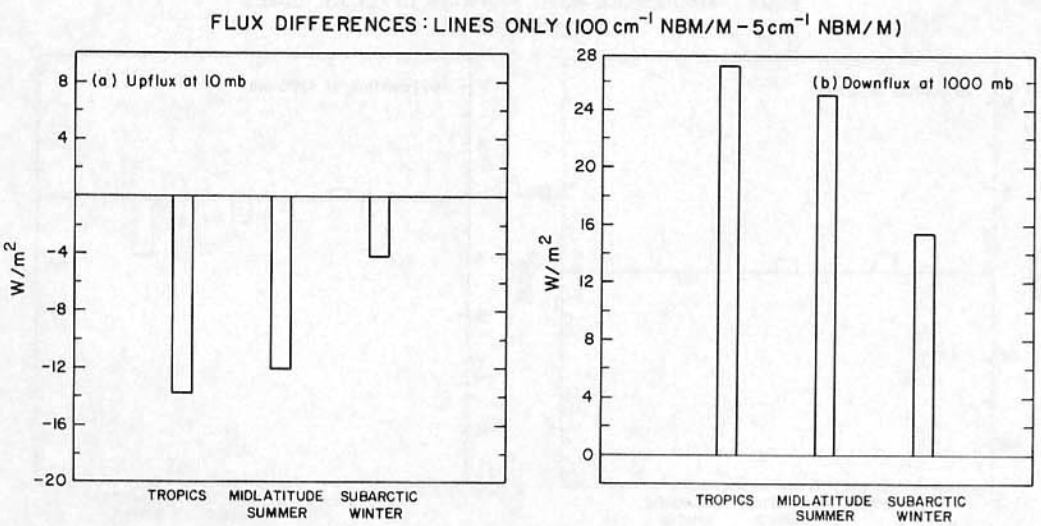

Fig. 13. Flux differences between 100 cm^{-1} NBM/M and 5 cm^{-1} NBM/M models. (*a*) Upflux at 10 mbar. (*b*) Downflux at 1000 mbar.

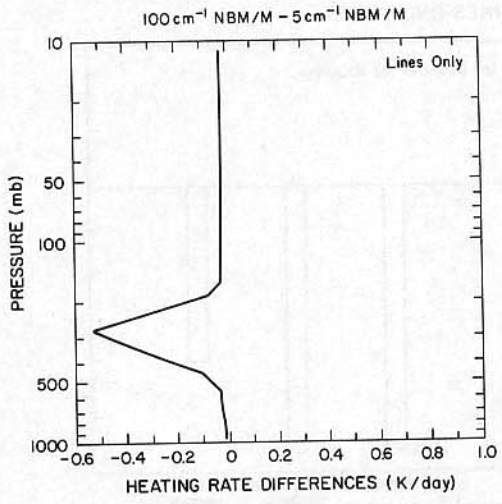

Fig. 14. Heating rate differences between 100 cm^{-1} NBM/M and 5 cm^{-1} NBM/M models for the mid-latitude summer atmosphere.

for treating the *e*-type absorption as well as the broadband overlap treatment between the lines and the *e*-type absorption introduces a maximum error of 1.5 W m^{-2} (for example, subtract bar in Figure 8*b* from that in Figure 8*a* for the subarctic summer profile).

7. Similar conclusions can be inferred from Table 3, which compares the *e*-type effects between NBM/M and EMIS.

In summary, the maximum error in the emissivity scheme is about 1% in the upflux at 50 km, about 1.5% in the downflux at the surface, and about 3% in the atmospheric-cooling rates.

4.3. *Comparison on a GCM Grid*

Up to this point the comparison was restricted to observed atmospheric profiles under clear-sky conditions. This is not sufficient to assess the accuracy of the scheme in a GCM which at any one time step can generate extreme combinations of temperatures and humidities unlike those encountered in the atmosphere. Furthermore, the accuracy has to be ascertained in the presence of clouds. Hence it is important to repeat the earlier comparison employing GCM simulations of temperatures, humidities and clouds.

For this purpose, both the emissivity and NBM/M models were introduced in the NCAR GCM known as the Community Climate Model. The CCM is described in detail by *Pitcher et al.* [1983] and by *Ramanathan et al.* [1983]. The radiative calculations employ the atmospheric conditions for day 200 of a perpetual January simulation described in *Ramanathan et al.* [1983]. The CCM has nine vertical levels from surface to 9 mbar, 48 equally spaced longitude points around a latitude circle and 40 latitude points from the south pole to the north pole. Hence 1920 vertical profiles are included in the comparison. The calculations also include the effects of CO_2 and O_3. In order to isolate the errors in the H_2O emissivity treatment, both the narrow-band (NBM/M) and the emissivity calculations employ the same band model treatment for CO_2 and O_3 and the same broadband overlap treatment for the overlap of CO_2 and O_3 bands with those of H_2O. The calculations also employ a nine-level cloudiness prescription.

The differences between the emissivity and the NBM/M model in the computed long-wave heating rates are shown in Figure 10. The results are shown for zonal mean heating rates only. The vertical distribution of the error displayed in Figure 10 is similar to that shown in Figure 6, that is, maximum error of the order of 0.15 K/day occurs close to the surface. However, the 0.15 K/day error is restricted to the latitude band between 10°–30°S. The percentage error is generally within 3% for all latitudes and altitudes. However, on a regional basis, for a few of the grid points (roughly 5% of the 1920 points) the error can be larger than the zonal mean error by a factor of 2 to 3. For example, at the lowest model level ($P = 991$ mbar) the maximum error at a few of the grid points is ± 0.4 K/day but the percentage error is only about 5%.

4.4. *Comparison With Line-by-Line Calculations and the Effect of the Far Wing Correction*

In order to ascertain the accuracy of the reference model used for the emissivity scheme, we compare the NBM/M and EMIS models with available line-by-line calculations. Several LBL calculations were cited in a recent international report *World Meteorological Organization* (*WMO*) [1984]. For our study, we chose the LBL results of A. Arking (private com-

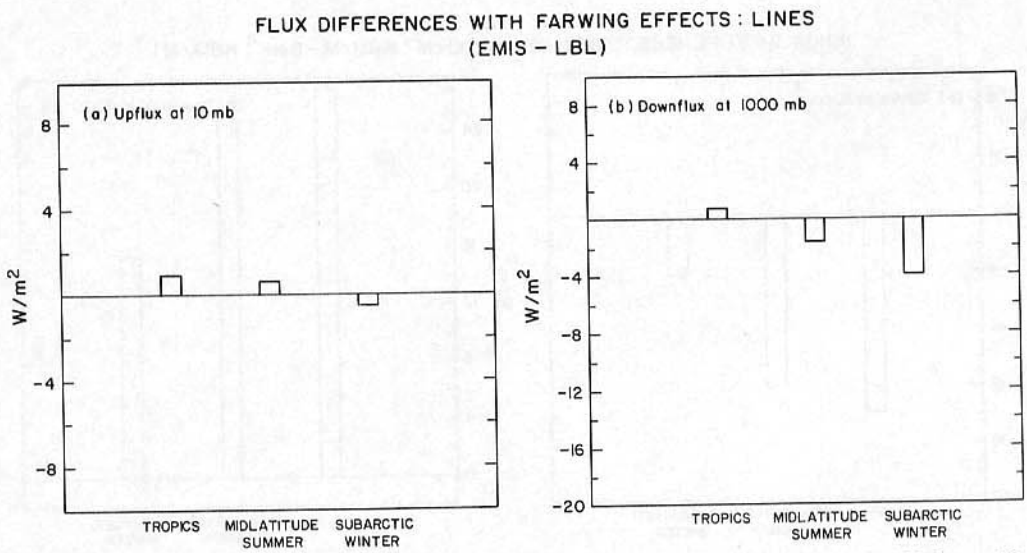

Fig. 15. Differences in fluxes between EMIS and LBL. The EMIS model includes far wing effects. (*a*) Upflux at 10 mbar. (*b*) Downflux at 1000 mbar.

TABLE 4*a*. Comparison of Fluxes With Line-by-Line Calculations, Lines Only, Uncorrected for Differences in the Spectral Domain Between the Various Models

Model	Spectral Domain, cm^{-1}	Upflux (0 mbar)	Downflux (1000 mbar)
LBL (A. Arking)	0–3000	336.52	260.31
LBL (S. B. Fels)	0–2200	333.96	263.8
EMIS (with far wing)		337.1	258.6
Surface emission	0–∞		
Atmospheric emission	0–2200		

Values are in watts per square meter. Far wing effects are included.

munication, 1985), reported as GLAS model by *WMO* [1984] and that of S. B. Fels (private communication, 1985), reported as GFDL model in *WMO* [1984], since these authors kindly provided us with the computer output of their results. In any case, as summarized by *WMO* [1984], the various LBL models agreed within 1% in the computed fluxes. The LBL models also adopt the empirical *e*-type continuum but do not include the *p*-type continuum. It is not entirely clear whether or not LBL models should include the *p*-type continuum. However, *Burch* [1982], in attempting to explain his laboratory data, accounts for transmission due to lines and finds that the *p*-type continuum absorption is needed to explain the observed transmission. This would imply that even LBL models which generally allow the Lorentzian lines to extend only about 10–20 cm^{-1} from the line centers (see Table 1 of *WMO* [1984]) should include the experimental *p*-type continuum. For the purpose of this comparison we remove the *p*-type absorption from the present NBM and EMIS models.

The difference between the NBM/M and LBL model in the upflux at 10 mbar is shown in Figure 11. The 5 cm^{-1} NBM model consistently overestimates the upflux. By comparing Figure 11*a* with Figure 11*b* it is seen that the inclusion of the *e*-type continuum masks the error but still the error is large. Figure 12 shows the difference between EMIS and LBL model for upflux at 10 mbar (Figure 12*a*) and for downflux at 1000 mbar (Figure 12*b*). The error in the upflux is consistent with that shown for the NBM model (Figure 11*a*). The overestimation of the upflux and the underestimation of the downflux clearly suggests that the 5 cm^{-1} model underestimates the opacity of the atmosphere. This underestimation is due to the implicit neglect of far wing effects in the 5 cm^{-1} model. For example, when we increase the spectral resolution from 5 to 100 cm^{-1}, the opacity of the atmosphere is significantly overestimated. This is illustrated in Figure 13, which displays the flux differences between the 100 and 5 cm^{-1} models. With increased resolution the upflux decreases by a significant amount, whereas the downflux increases by a significant amount. *Morcrette and Fouquart* [1985] have independently obtained results similar to those shown in Figure 13. Thus the spectral resolution in a narrow-band model is an arbitrary parameter. The differences in the cooling rates between the 100 and 5 cm^{-1} models for the mid-latitude summer profile are shown in Figure 14. In this study we adopt emissivity based on the 5 cm^{-1} model, but as mentioned earlier, incorporate a far wing opacity to bring the emissivity scheme into agreement with the LBL calculation.

TABLE 4*b*. Comparison of Fluxes With LBL Calculations, Lines Only, Corrected for Differences in the Spectral Domain

Model	Spectral Domain, cm^{-1}	Upflux (0 mbar)	Downflux (1000 mbar)
LBL (A. Arking)	0–2200	334.4	260.13
LBL (S. B. Fels)	0–2200	333.96	263.8
EMIS (with far wing)		335	258.6

Values are in watts per square meter. Far wing effects are included.

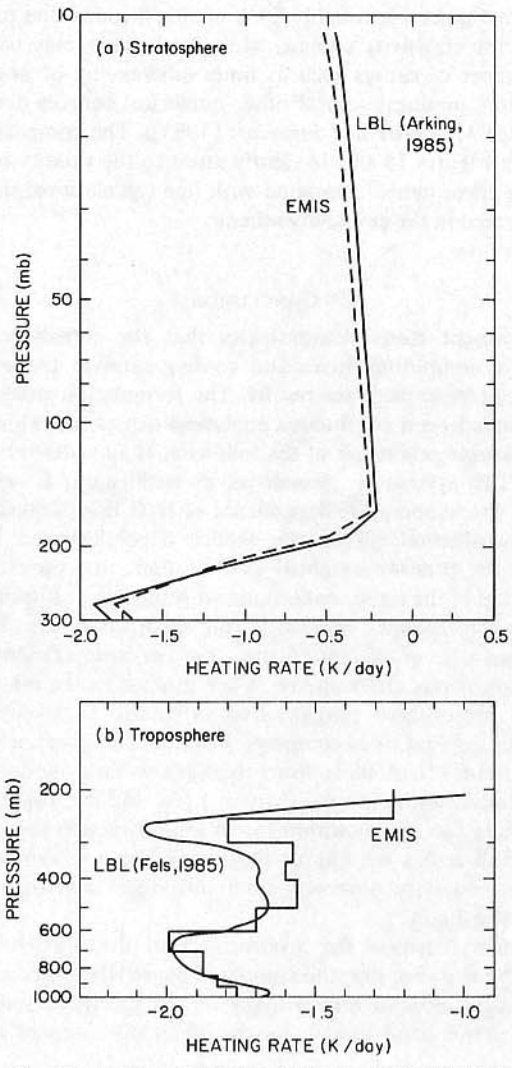

Fig. 16. Comparison of heating rates as computed by the emissivity scheme with far wing effects and line-by-line calculations: (*a*) stratosphere and (*b*) troposphere. EMIS denotes emissivity model and LBL denotes line-by-line calculations.

With the inclusion of the far wing opacity, as given by equations (32) to (34), the emissivity scheme is in excellent agreement with the LBL calculations as shown in Figure 15 and Tables 4*a* and 4*b*. The heating rates generated by the emissivity scheme and the LBL scheme are compared in Figure 16 for the mid-latitude summer atmosphere profile. The heating rate differences for other atmospheric profiles are either similar to or smaller than those shown in Figure 16. For the troposphere we chose S. B. Fels' (private communication, 1985) calculations because of the high vertical resolution (20-mbar-thick layers) in Fels' model, whereas for the stratosphere the Arking model (A. Arking, private communication, 1985) is chosen, since Arking's model has a better vertical resolution than Fels' model for the stratosphere. The maximum error in the heating rate is about 0.22 K/day, and based on the results

shown in Figure 16, roughly 50% of this error is due to the error in the emissivity scheme, while the balance may be due to a number of causes such as finite differencing or angular integration, amongst several other numerical sources (for example, see *Morcrette and Fouquart* [1985]). The comparisons shown in Figures 15 and 16 clearly attest to the validity of the far wing effect (when compared with line calculations) that is incorporated in the emissivity scheme.

5. Conclusion

The present study demonstrates that the emissivity approach of computing fluxes and cooling rates in the atmosphere can yield accurate results. The formulation proposed here is based on a continuous analytical expression which at the same time retains all of the following H_2O radiative processes: The asymptotic properties at pathlength, $U \to 0$ to $U \to \infty$; the temperature dependence of H_2O line parameters; the nonisothermal effects; the explicit dependence on H_2O amount, the pressure-weighted H_2O amount, and on e^2; and the overlap of the e-type continuum with the line absorption.

The nonisothermal emissivity and absorptivity are developed from a set of reference 5 cm^{-1} narrow-band calculations for homogeneous atmospheres. When applied to the inhomogeneous atmosphere ranging from antarctic to tropics to arctic, the cooling rates computed from the emissivity scheme agree within 3% of those from the narrow-band model; the surface downward flux agrees within 1.5%, and the top-of-the-atmosphere flux agrees within 1%. A major fraction ($>1/2$) of these small errors are due to the strong-line approximation, and the emissivity approach itself introduces less than 1% error in the fluxes.

We then illustrate the arbitrariness of the narrow-band models by showing that the computed emissivities, fluxes, and cooling rates depend very strongly on the spectral resolution of the narrow-band model. Furthermore, we compare the 5 cm^{-1} narrow-band model results with LBL calculations and conclude that the 5 cm^{-1} model underestimates the opacity due to far wings of the rotational lines. Hence we incorporate a far wing continuum-type opacity in the emissivity scheme to bring it to excellent agreement with LBL calculations.

This study thus demonstrates that the H_2O radiative effects in the atmosphere can be modeled accurately by the emissivity approach proposed in this study.

Appendix

The analytical expressions for emissivity E and absorptivity A are given in Table A1. The expressions for the line transmission tl and the continuum transmission tc are given in Table A2. In what follows we will describe the procedure adopted for parameterizing the effective absorption coefficient kl (see equation (20) in the text), for the rotation and the vibration-rotation band.

The functional dependence of kl can be written as:

$$kl(u, Te, Tp) = kl_\infty(Te, Tp) + \{\delta kl/(1. + [\delta klC(U^{1/2})]\} \quad \text{(A1)}$$

$$\delta kl = kl_0(Te, Tp) - kl_\infty(Te, Tp) \quad \text{(A2)}$$

$$C = C(U, Te, Tp) \quad \text{(A3)}$$

Equation (A1) satisfies the following limits:

$$kl \to kl_\infty \qquad U \gg 1 \quad \text{(A4)}$$

$$kl \to kl_0 \qquad U \ll 1 \quad \text{(A5)}$$

The kl_0 is estimated by letting $U \to 0$ in the reference emissivity equation (16) and in the parameterized emissivity equation (17). The resulting asymptotic expressions of (16) (with the aid of equation (14)) and (17) are matched in conjunction with (A5) for the definition of kl_0, which yields:

$$kl_0(Te, Tp) = \left[\sum_{i=1}^{N} B_i(1.66k_i\beta_i)^{1/2}\right] \Big/ \left[\sum_{i=1}^{N} B_i\right] \quad \text{(A6)}$$

TABLE A1. Analytical Expressions for Emissivity and Absorptivity

Item	Equation	Comments
	Total Emissivity	
$E = \sum_{j=1} E_j$	(1)	
	$j = 1$, 0–800 cm^{-1}: *Pure-Rotation Band*	
$E_1 = f[1. - tl]$	(2)	tl is effective line transmission
$f(Te) = \left[\int_{\omega_1}^{\omega_2} B_\omega\, d\omega/B\right]$	(3)	f is fraction of blackbody energy in the interval of interest; $\omega_1 = 0$; $\omega_2 = 800$ cm^{-1}
	$j = 2$, 500–800 cm^{-1}: *Continuum With Line Overlap*	
$E_2 = f\left\{\sum_{i=1}^{2} 0.5tl(i)[1 - tc(i)]\right\}$	(4)	i denotes subinterval; tc is continuum transmission; tl accounts for line overlap
	$j = 3$, 800–1200 cm^{-1}: *Continuum Plus Lines*	
$E_3 = f\left\{\sum_{i=1}^{2} 0.5[1 - tl(i)tc(i)]\right\}$	(5)	
	$j = 4$, 1200–2200 cm^{-1}: *Vibration-Rotation Band**	
		same as equation (2) for E_1
	Total Absorptivity	
$A = \sum_{j=1}^{4} Aj$	(6)	equations for A_1 to A_4 are identical to those for E_1 to E_4 except replace B_ω and B with dB_ω/dT and dB/dT

TABLE A2. Expressions for Transmission

Item	Band Interval, cm^{-1}	Expression	Equation	Comments
Lines	0–800; 1200–2200	$tl = \exp\{-kl[(U^{1/2}) + GU]\}$	(1)	$kl(U, Te, Tp)$
		$U = \int (P/P_0)\, dW^*$	(2)	$P_0 = 1$ atm
		$W = \int \rho_w\, dz^*$	(3)	$\rho_w = H_2O$ density
				see (33) in text for G
Continuum plus line overlap	500–800	$tc(i) = \exp\{-kc(i)[Y + 0.0017\, U]\}$	(4)	$i = 1$ is 650–800 cm^{-1}, $i = 2$ is 500–650 cm^{-1},
		$kc(1) = \overline{kc}$; $kc(2) = 2\overline{kc}$	(5)	see Table A3 for $\overline{kc}$
		$tl(i) = \exp\{-kl(i)[(U^{1/2}) + GU]\}$	(6)	see (34) in text for G
		$Y = \int (e/P_0) \exp\{1800[(1/Tp) - (1/296)]\}\, dW$	(7)	$e = H_2O$ partial pressure
Continuum plus lines	800–1200	$tc(i) = \exp\{-kc(i)[Y + 0.002U]\}$	(8)	$i = 1$ is 1000–1200 cm^{-1}
		$kc(1) = \overline{kc}$; $kc(2) = 2\overline{kc}$	(9)	$i = 2$ is 800–1000 cm^{-1}
		$tl(i) = \exp\{-(k_i\bar{P}_i/2\beta_i)[(1 + c4\beta_i\bar{W}_i/\bar{P}_i)^{1/2} - 1]\}$	(10)	$\bar{W}_i = 1.66W\Phi_i$; $\bar{P}_i = U/W\ \Psi_i/\Phi_i$; k_i and β_i are defined in Table A6
		$c = 0.61 + [0.39/(1. + 10\bar{W}_i\bar{P}_i)]$	(11)	

The values Φ_i and Ψ_i account for the temperature dependence of line parameters, as given by *Rodgers* [1967] (See Table A3). Te, emitting level temperature; Tp, path length temperature.

*Values given in grams per square centimeter.

The kl_0, as defined by (A6), is basically the Planck-function-weighted strong-line coefficient that is analogous to the Planck mean coefficient [*Sparrow and Cess*, 1968] derived for the optically thin limit. Note that kl_0 is independent of U but depends on Te and Tp. The other asymptotic parameter kl_∞ basically represents the contribution from the weakest lines and is obtained by estimating kl from (20) for $U \gg 1$ (in grams per square centimeter), and for this purpose U is chosen to be 10^4 g cm^{-2}. The correction factor C contributes a maximum of 10% to kl and furthermore it does not influence the asymptotic properties of E. Analytical expressions for C are given in Table A3*b* and the constants for computing C are given in Table A3*c*. For all values of U, Te, and Tp, kl, as defined in (A1), fits the computed value of kl (equation (20)) within 1%, while without the correction factor C, the error is about 5%. Additional description of C is given in Tables A3*a* and A3*b*.

The final issue is to formulate the dependence on Te and Tp. First we let

$$V(Te, Tp) = V(Te)V(Tp) \tag{A7}$$

where V denotes either kl_∞, kl_0, or C. As implied by (A7), it is assumed that the dependence on Te is separable from that on Tp. The two functions are evaluated by letting

$$V(Te) = V(Te, Tp = 250\ \text{K}) \tag{A8}$$

$$V(Tp) = V(Te, Tp = Te)/V(Te, Tp = 250\ \text{K}) \tag{A9}$$

For example, $kl(U, Te)$ is computed from (20) by setting $Tp = 250$ K for the E(REF) computations. For $kl(U, Tp)$ the numerator in (A9) is evaluated from (20) by setting $Tp = Te$ in the E(REF) computations. The only justification for (A7) to (A9) is that they seem to work. We caution the reader against back-substitution of A9 and A8 into A7 and erroneously con-

TABLE A3*a*. Parametric Expressions for the Parameters Defined in Tables A1 and A2

Parameter	Expression	Equation	Comments
f	$a_0 + a_1\Delta Te + a_2\Delta Te^2 + \cdots$	(1)	all spectral intervals
kl	$kl_\infty + \dfrac{\delta kl}{1 + C\ \delta kl(U^{1/2})}$	(2)	0–800 cm^{-1}; 1200–2200 cm^{-1} only
kl_∞	$a_\infty(Te)a_\infty(Tp)$	(3)	
δkl	$\delta a(Te)\delta a(Tp)$	(4)	
$a_\infty(Te)$	$a_0 + a_1\Delta Te + a_2\Delta Te^2 + \cdots$	(5)	
$a_\infty(Tp)$	$a_0 + a_1\Delta Tp + a_2\Delta Tp^2 + \cdots$	(6)	$\delta a(Te)$ and $\delta a(Tp)$ are similar to (5) and (6) above
$\dfrac{C}{\overline{kc}}$	$(1. + 2Y/1. + 15Y)(a_0 + a_1\Delta Te)$	(7)	see Table A3*a* 500–800 cm^{-1}
$kl(i)$	$kl_\infty(i) + \dfrac{\delta kl(i)}{1. + CF(i)(U^{1/2})}$	(8)	$i = 1$ is 650–800 cm^{-1}; $i = 2$ is 500–650 cm^{-1}; kl_∞ and δkl are as in (3) to (6) but independent of Te
$CF(1)$	0.1 + 3.E-5*$(Tp - 260)^2$	(9)	
$CF(2)$	0.5 + 2.053E-3 $(Tp - 260)$	(10)	
Φ_i	$\exp(a_1\Delta Tp + a_2\Delta Tp^2)$	(11)	$i = 1$ is 1000–1200 cm^{-1}; $i = 2$ is 800–1000 cm^{-1}
$\dfrac{\Psi_i}{\overline{kc}}$	$\exp(b_1\Delta Tp + b_2\Delta Tp^2)$	(12)	800–1200 cm^{-1}
	$a_0 + a_1\Delta Te$	(13)	

The numerical constants are given in Tables A4*a*, A4*b*, A5, and A6. $\Delta Te = Te - TR$; $\Delta Tp = Tp - TR$; TR is the reference temperature.

*Read 3.E-5 as $3. \times 10^{-5}$.

TABLE A3*b*. Correction Factors, Expressions Only

Parameter	Expression
	Rotation Band Emissivity
$C(U, T)$	$A_3(A_1 + A_2)$
A_3	$a_0 + a_1\Delta Tp + a_2\Delta Tp^2$
A_1	$a_0 + a_1\Delta Te + a_2\Delta Te^2$
A_2	$\dfrac{(a_0 + a_1\Delta Te + a_2\Delta Te^2)(b_0 + b_1\Delta Tp + b_2\Delta Tp^2)}{0.9 + 2.62(U^{1/2})}$
	Rotation Band Absorptivity
$C(U, T)$	$A_3(A_1 + A_2)$
A_3	$a_0 + a_1\Delta Tp + a_2\Delta Tp^2$
A_1	$a_0 + a_1\Delta Te + a_2\Delta Te^2$
A_2	$\dfrac{2.(a_0 + a_1\Delta Te + a_2\Delta Te^2)(b_0 + b_1\Delta Tp + b_2\Delta Tp^2)}{1 + 3.6(U^{1/2})}$
	Vibration-Rotation Band
$C(U, T)$	$A_1\ A_2\ A_3$
A_1	0.30
A_2	$1. + \dfrac{a_0 + a_1\Delta Te}{1. + 1.3(U^{1/2})}$
A_3	$a_0 + a_1\Delta Tp + a_2\Delta Tp^2$
	Vibration-Rotation Band Absorptivity
$C(U, T)$	$A_1\ A_2\ A_3$ where
A_1	0.29
A_2	$1. + \dfrac{a_0 + a_1\Delta Te}{1. + 1.3(U^{1/2})}$
A_3	$a_0 + a_1\Delta Tp + a_2\Delta Tp^2$

cluding that $V(Te, Tp) = V(Te, Te)$. Equations A8 and A9 are simply a technique to extract the dependence of V separately on Te and Tp. The values are estimated for U, ranging from 10^{-6} to 10^4 g cm^{-2}, and for T, ranging from 160 to 320 K. A similar procedure is adopted for kl_0, kl_∞, and C.

The empirical expressions for f, kl, and kc are given in Table A3*a*. The constants for kl and f are given in Tables A4*a* and A4*b* for the rotational and the vibration-rotation band and those for the continuum regions, 500–800 cm^{-1} and 800–1200 cm^{-1}, are given in Tables A5 and A6, respectively.

TABLE A3*c*. Constants to Calculate the Correction Factors

Terms	a_0	a_1	a_2	b_0	b_1	b_2	ΔT
			Rotation Band: Emissivity				
A_1	0.37	−3.33E − 5*	3.33E − 6				*Te*-300
A_2	1.387	3.80E − 3	−7.8E − 6				*Te*-300
A_2				1.	−1.21E − 3	−5.33E − 6	*Tp*-300
A_3	1.07	−1.00E − 3	1.475E − 5				*Tp*-300
			Rotation Band: Absorptivity				
A_1	0.44	3.38E − 4	−1.52E − 6				*Te*-300
A_2	1.	1.717E − 3	−1.133E − 5				*Te*-300
A_2				1.	4.443E − 3	2.75E − 5	*Tp*-300
A_3	1.05	−6.00E − 3	3.E − 6				*Tp*-300
			Vibration-Rotation Band: Emissivity				
A_1	0.3						
A_2	1.75	−3.96E − 3					*Te*-300
A_3	1.	1.25E − 3	6.25E − 5				*Tp*-300
			Vibration-Rotation Band: Absorptivity				
A_1	0.29						
A_2	1.75	−3.96E − 3					*Te*-300
A_3	1.	1.25E − 3	6.25E − 5				*Tp*-300

*Read −3.33 E − 5 as -3.33×10^{-5}.

TABLE A4*a*. Coefficients for Calculating *kl* and *f* for Emissivity

	a_0	a_1	a_2	a_3	ΔT
		Rotation Band (0–800 cm^{-1})			
$a_\infty(Tp)$	1.01400E + 0*	6.41695E − 3	2.85787E − 5		*Tp*-250
$a_\infty(Te)$	3.93137E − 2	−4.34341E − 5	3.74545E − 7		*Te*-250
$\delta a(Tp)$	9.90127E − 1	1.22475E − 3	4.90135E − 6		*Tp*-250
$\delta a(Te)$	8.85675E + 0	−3.51620E − 2	2.38653E − 4	−1.71439E − 6	*Te*-250
$f(Te)$	7.03047E − 1	−2.63501E − 3	−1.57023E − 6		*Te*-250
		Vibration-Rotation Band (1200–2200 cm^{-1})			
$a_\infty(Tp)$	1.02920E + 0	1.01680E − 2	5.30226E − 5		*Tp*-250
$a_\infty(Te)$	7.42500E − 2	3.97397E − 5			*Te*-250
$\delta a(Tp)$	9.75230E − 1	1.03341E − 3			*Tp*-250
$\delta a(Te)$	6.64034E + 0	1.56651E − 2	−9.73357E − 5		*Te*-250
$f(Te)$	7.88193E − 2	1.31290E − 3	4.25827E − 6	−1.23982E − 8	*Te*-250

*Read 1.01400E + 0 as 1.01400×10^0.

TABLE A4*b*. Coefficients for Calculating *kl* and *f* for Absorptivity

	a_0	a_1	a_2	a_3	ΔT
		Rotation Band (0–800 cm^{-1})			
$a_\infty(Tp)$	1.01320E + 0*	6.86400E − 3	2.96961E − 5		*Tp*-250
$a_\infty(Te)$	3.67785E − 2	−3.10794E − 5	2.94436E − 7		*Te*-250
$\delta a(Te)$	9.89753E − 1	1.97081E − 3	3.42046E − 6		*Tp*-250
$\delta a(Te)$	5.73841E + 0	−1.91919E − 2	1.65993E − 4	−1.54665E − 6	*Te*-250
$f(Te)$	5.29269E − 1	−3.14754E − 3	4.39595E − 6		*Te*-250
		Vibration-Rotation Band (1200–2200 cm^{-1})			
$a_\infty(Tp)$	1.02743E + 0	9.85113E − 3	5.00233E − 5		*Tp*-250
$a_\infty(Te)$	7.52859E − 2	4.18073E − 5			*Te*-250
$\delta a(Tp)$	9.77366E − 1	8.60014E − 4			*Tp*-250
$\delta a(Te)$	7.09281E + 0	1.40056E − 2	−1.15774E − 4		*Te*-250
$f(Te)$	1.62744E − 1	2.22847E − 3	2.60102E − 6	−4.30133E − 8	*Te*-250

*Read 1.01320E + 0 as 1.01320×10^0.

TABLE A5. Continuum and Line Parameters for the 500–800 cm^{-1} Spectral Region

	a_0	a_1	a_2	a_3	a_4	a_5	ΔT
			Continuum Band: Emissivity				
$\overline{kc}(Te)$	5.46557E + 1*	−7.30387E − 2					$Te - 250$
f	3.31654E − 1	−2.86103E − 4	−7.87860E − 6	5.88187E − 8	−1.25340E − 10	−1.37731E − 12	$Te - 250$
			Continuum Band: Absorptivity				
$\overline{kc}(Te)$	5.11479E + 1	−6.82615E − 2					$Te - 250$
f	3.14365E − 1	−1.33872E − 3	−2.15585E − 6	6.07798E − 8	−3.45612E − 10	−9.34139E − 15	$Te - 250$
			Parameters for the Rotation Band: Transmissivity				
a_∞ for $kl_\infty(1)$	2.82096E − 2	2.47836E − 4	1.16904E − 6				$Tp - 250$
a_∞ for $kl_\infty(2)$	9.27379E − 2	8.04454E − 4	6.88844E − 6				$Tp - 250$
δa for $kl(1)$	2.48852E − 1	2.09667E − 3	2.60377E − 6				$Tp - 250$
δa for $kl(2)$	1.03594E + 0	6.58620E − 3	4.04456E − 6				$Tp - 250$

*Read 5.46557E + 1 as 5.4655×10^1.

TABLE A6. Band Parameters for 800–1200 cm^{-1}

	a_0	a_1	a_2	a_3	a_4	a_5	ΔT
			Emissivity				
$\overline{kc}(Te)$	9.04489E + 0*	−9.56499E − 3					$Te - 250$
f	2.20370E − 1	1.39719E − 3	−7.32011E − 6	−1.40262E − 8	2.13638E − 10	−2.35955E − 13	$Te - 250$
			Absorptivity				
$\overline{kc}(Te)$	8.72239E + 0	−9.53359E − 3					$Te - 250$
f	3.07431E − 1	8.27225E − 4	−1.30067E − 5	3.49847E − 8	2.07835E − 10	−1.98937E − 12	$Te - 250$
$\Delta\omega$ cm^{-1}	k_i	β_i	a_1	a_2	b_1	b_2	ΔT
			Rotational Line Transmission, tl(i)				
800–1000	2.3674E − 2	3.9747E − 1	2.88E − 2	−5.8E − 5	2.99E − 2	−8.63E − 5	$Tp - 235$
1000–1200	8.7469E − 2	1.2198	2.32E − 2	−9.51E − 5	2.17E − 2	−7.85E − 5	$Tp - 235$

See equation (10) of Table A2 and equations (11) and (12) of Table A3 for rotational line transmission.
*Read 9.04489E + 0 as 9.04489×10^0.

Acknowledgments. We are indebted to J. T. Kiehl for numerous discussions and suggestions with regard to the narrow band calculations reported here. We benefited immensely by participating in an international radiation model intercomparison study organized by F. Luther and Y. Fouquart. As participants in this study, A. Arking and S. B. Fels generously shared with us the results of their line-by-line calculations, which helped us identify deficiencies in an earlier version of our scheme. We thank S. B. Fels, J. J. Morcrette, J. A. Coakley, R. E. Dickinson and the two anonymous reviewers for their valuable comments on the manuscript. This work constitutes a part of our efforts in the NASA Earth Radiation Budget Experiment Program and we thank the NASA Langley Research Center for partial support of this work through grant L9477B. Part of this work was completed when one of us (V.R.) was on a sabbatical leave at NASA Langley Research Center in Hampton, Virginia, and thanks are due to the Atmospheric Sciences Division of NASA Langley for the hospitality. We thank G. Escobar for her help in preparation of this manuscript. The National Center for Atmospheric Research is sponsored by the National Science Foundation.

REFERENCES

Burch, D. E., Continuum absorption by H_2O, final report, p. 46, Air Force Geophy. Lab., Hanscom Air Force Base, Mass., 1982.

Cess, R. D., Radiative transfer due to atmospheric water vapor: Global considerations of the earth's energy balance, *J. Quant. Spectrosc. Radiat. Transfer*, *14*, 861–872, 1974.

Chou, M-D., and A. Arking, Computation of infrared cooling rates in the water vapor bands, *J. Atmos. Sci.*, *37*, 855–867, 1980.

Coakley, J. A., and B. P. Briegleb, Accurate calculations of fluxes and cooling rates using emissivities, paper presented at Third Conference on Atmospheric Radiation, Am. Meteorol. Soc., June 28–30, Univ. of Calif., Davis, 1978.

Fels, S. B., and D. Schwarzkopf, The simplified exchange approximation: A new method for radiative transfer calculations, *J. Atmos. Sci.*, *32*, 1475–1488, 1975.

Garand, L., Some improvements and complements to the infrared emissivity algorithm including a parameterization of the absorption in the continuum region, *J. Atmos. Sci.*, *40*, 230–244, 1983.

Goody, R. M., A statistical model for water-vapour absorption, *Q. J. R. Meteorol. Soc.*, *78*, 165–169, 1952.

Kiehl, J. T., and V. Ramanathan, CO_2 radiative parameterization used in climate models: Comparison with narrow band models and with laboratory data, *J. Geophys. Res.*, *88*, 5191–5202, 1983.

Kneizys, F. S., E. P. Shettle, W. O. Gallery, J. H. Chetwynd, Jr., L. W. Abrew, J. E. A. Selby, R. W. Fenn, R. A. McClatchey, Atmospheric transmittance/radiance: Computer code LOWTRAN 5, *Tech. Rep. AFGL-TR-80-0067*, p. 9, Air Force Geophys. Lab., Hanscom Air Force Base, Mass., 1980.

Liou, K. N., and S. S. Ou, Parameterization of infrared radiative transfer in cloudy atmospheres, *J. Atmos. Sci.*, *38*, 2707–2716, 1981.

Liou, K. N., and S. S. Ou, Theory of equilibrium temperature in radiative-turbulent atmospheres, *J. Atmos. Sci.*, *40*, 215–229, 1983.

Malkmus, W., Random Lorentz band model with exponential-tailed s^{-1} line intensity distribution function, *J. Opt. Soc. Am.*, *57*, 323–329, 1967.

Manabe, S., and R. T. Wetherald, Thermal equilibrium of the atmosphere with a given distribution of relative humidity, *J. Atmos. Sci.*, *24*, 241–259, 1967.

McClatchey, R. A., R. W. Fenn, J. E. A. Selby, F. E. Volz, and J. S. Garing, Optical properties of the atmosphere, 3rd ed., *Rep. AFCRL-72-0497*, 108 pp., 1972. (Doc. NTIS N7318412, may be obtained from Natl. Tech. Inf. Serv., Springfield, Va.)

Morcrette, J. J., and Y. Fouquart, On systematic errors in parameterized calculations of longwave radiation transfer, *Q. J. R. Meteorol. Soc.*, *111*, 691–708, 1985.

Pitcher, E. J., R. C. Malone, V. Ramanathan, M. L. Blackmon, K. Puri, and W. Bourke, January and July simulations with a spectral general circulation model, *J. Atmos. Sci.*, *40*, 580–604, 1983.

Ramanathan, V., Radiative transfer within the earth's troposphere and stratosphere: A simplified radiative-convective model, *J. Atmos. Sci.*, *33*, 1330–1346, 1976.

Ramanathan, V., E. J. Pitcher, R. C. Malone, and M. L. Blackmon, The response of a spectral general circulation model to refinements in radiative processes, *J. Atmos. Sci.*, *40*, 605–630, 1983.

Roberts, R. E., J. E. A. Selby, and L. M. Biberman, Infrared continuum absorption by atmospheric water vapor in the 8–12 μm window, *Appl. Opt.*, *15*, 2085–2090, 1976.

Rodgers, C. D., The use of emissivity in atmospheric radiation calculations, *Q. J. R. Meteorol. Soc.*, *93*, 43–54, 1967.

Rodgers, C. D., and D. C. Walshaw, The computation of infrared cooling rate in planetary atmosphere, *Q. J. R. Meteorol. Soc.*, *92*, 67–92, 1966.

Rothman, L. S., AFGL atmospheric absorption line parameters, Compilation: 1980 version, *Appl. Opt.*, *20*, 791–795, 1981.

Rothman, L. S., R. R. Gamache, A. Barbe, A. Goldman, J. R. Gillis, L. R. Brown, R. A. Toth, J.-M. Flaud and C. Camy-Peyret, AFGL atmospheric absorption line parameters compilation: 1982 edition. *Appl. Opt.*, *22*, 2247–2256, 1983.

Sasamori, T., The radiative cooling calculation for application to general circulation experiments, *J. Appl. Meteorol.*, *7*, 721–729, 1968.

Sparrow, E. M., and R. D. Cess, Radiation heat transfer, p. 366, McGraw-Hill, New York, 1970.

Staley, D. O., and G. N. Jurica, Flux emissivity tables for water vapor, carbon dioxide and ozone, *J. Appl. Meteorol.*, *9*, 365–372, 1970.

World Meteorological Organization, The intercomparison of radiation codes in climate models, edited by F. M. Luther and Yves Fouquart, *World Climate Prog. Rep. WCP-93*, 37 pp. Geneva, 1984.

P. Downey, National Center for Atmospheric Research, P. O. Box 3000, Boulder, CO 80307.

V. Ramanathan, Department of Geophysics, University of Chicago, 5734 S. Ellis Avenue, Chicago, Ill., 60637.

(Received January 30, 1985;
revised March 24, 1986;
accepted April 1, 1986.)